

# Hairy black holes induced by nonlinear superradiant instability

Cheng-Yong Zhang,<sup>1,\*</sup> Qian Chen,<sup>2,†</sup> Yuxuan Liu,<sup>3,‡</sup> Yu Tian,<sup>2,4,§</sup> and Bin Wang<sup>5,6,¶</sup>

<sup>1</sup>*Department of Physics and Siyuan Laboratory, Jinan University, Guangzhou 510632, China*

<sup>2</sup>*School of Physical Sciences, University of Chinese Academy of Sciences, Beijing 100049, China*

<sup>3</sup>*Affiliation: School of Physics and Electronics, Central South University, Changsha 410003, China*

<sup>4</sup>*Institute of Theoretical Physics, Chinese Academy of Sciences, Beijing 100190, China*

<sup>5</sup>*Center for Gravitation and Cosmology, College of Physical Science  
and Technology, Yangzhou University, Yangzhou 225009, China*

<sup>6</sup>*School of Aeronautics and Astronautics, Shanghai Jiao Tong University, Shanghai 200240, China*

We unveil a new insight: beyond linear superradiant instability, a nonlinear mechanism can transform linearly stable bald black holes into hairy ones in asymptotically flat spacetime without necessitating artificial mirrors. As an illustrative example, by perturbing Reissner-Nordström (RN) black holes with a complex scalar field featuring a physical Q-ball type potential, we discover that significant perturbations can destroy the stability of RN black holes, resulting in the formation of Q-hairy black holes through an innovative nonlinear superradiant instability. For the first time in a black hole system, we observe the scalar hair displaying rhythmic radial expansion and contraction, indicating a novel type of bosenova. We find critical solutions at transition thresholds between bald and hairy black holes, inducing distinctive dynamical critical behaviors stemming from an intricate linear instability inherent in the critical solution.

## I. INTRODUCTION

Superradiance arises from the interaction between rotating or charged black holes and their surrounding environments, amplifying radiation scattering from the black holes and extracting energy, angular momentum, and charge from them. It holds profound importance for black hole stability and dynamics [1]. When the amplified radiation is confined, it triggers superradiant instability, known as the “black hole bomb” [2], which has noteworthy implications for investigating dark matter and for probing physics beyond the Standard Model [3].

At the threshold of superradiant instability, the presence of zero modes or bound states often signals the emergence of new hairy black hole solutions. These solutions are well-explored in rotation scenarios, where synchronized massive free complex bosonic hair arises from Kerr black holes [4]. The synchronization condition ensures the hair persistence outside the horizon by inhibiting energy flux across it. However, in charged scenarios, RN black holes lack superradiant bound states or zero modes [5], obstructing the bifurcation of hairy black hole solutions from the RN solutions. Nonetheless, recent breakthroughs have introduced novel black hole solutions endowed with gauged massive self-interacting complex scalar Q-hair, fulfilling a resonance condition [6]. Diverging from being zero modes of the superradiant instability, these solutions exhibit a mass gap compared to the RN solutions. The self-interactions, mandatory for the hairy solutions, challenge Mayo and Bekenstein’s no-hair theo-

rem [7], while uphold the weak or dominant energy conditions and adhere to a physically meaningful Q-ball type potential [8, 9]. These findings collectively highlight that the basic electro-vacuum solutions in general relativity extend into minimally coupled bosonic hair [10].

While the linear aspects of superradiant instability regarding massive bosonic fields around rotating black holes are well understood, exploring its nonlinear progression is challenging due to the significant disparity in timescales between field oscillations and instability growth rates [11]. Some progress has been made in simulating the early stages of superradiant instability for vector fields, which have shorter instability timescales than scalar fields [12, 13], but further research is required to fully grasp the ultimate outcome [1]. In contrast, confined RN black holes in an artificial cavity or anti-de Sitter (AdS) space exhibit much faster growth rates, even with scalar fields [14]. Nonlinear simulations have shown that their superradiant instability ultimately results in black holes surrounded by harmonically oscillating scalar field condensates [15–18].

In this Letter, we reveal a novel insight: a nonlinear mechanism can transform stable bald black holes into hairy ones, beyond the linear superradiant stability that transforms unstable ones. As an illustrative example, we perform full nonlinear simulations of RN black holes surrounded by a complex scalar field with a physical Q-ball type potential. An intriguing facet of our investigation lies in the natural confinement mechanisms offered by the scalar field mass and self-interaction without violating energy conditions, eliminating the need for artificial mirrors or AdS boundaries. Our discoveries demonstrate that while RN black holes exhibit superradiance and remain stable against small perturbations, significant perturbations can trigger an innovative nonlinear instability. During the evolution, charge is extracted from the black hole, channeling entirely into the scalar field. This

\* [zhangcycy@email.jnu.edu.cn](mailto:zhangcycy@email.jnu.edu.cn)

† [chenqian192@mails.ucas.ac.cn](mailto:chenqian192@mails.ucas.ac.cn)

‡ [liuyuxuan@ucas.ac.cn](mailto:liuyuxuan@ucas.ac.cn)

§ [ytian@ucas.ac.cn](mailto:ytian@ucas.ac.cn)

¶ [wang\\_b@sjtu.edu.cn](mailto:wang_b@sjtu.edu.cn)

process accompanies rhythmic radial expansion and contraction of the scalar hair, persisting until the system settles into a stationary black hole adorned with Q-hair. Moreover, we discover novel dynamical critical behaviors at transition thresholds between bald and hairy black holes. These critical behaviors exhibit type I patterns due to an intricate linear instability inherent in the critical solutions, distinguishing them from those induced by tachyonic instability [19–22].

## II. MODEL

We consider the Einstein-Maxwell gravity minimally coupled with a self-interacting massive complex scalar  $\psi$ . The Lagrangian density is

$$\mathcal{L} = R - F_{\mu\nu}F^{\mu\nu} - D^\mu\psi(D_\mu\psi)^* - V(\psi), \quad (1)$$

where  $R$  represents the Ricci scalar associated with metric  $g_{\mu\nu}$ . The Maxwell field strength  $F_{\mu\nu} = \partial_\mu A_\nu - \partial_\nu A_\mu$ , where  $A_\mu$  is the gauge potential. The gauge covariant derivative  $D_\mu = \nabla_\mu - iqA_\mu$ , with  $q$  denoting the gauge coupling constant. We focus on the physical potential used in Q-ball literature [8, 9]:

$$V(\psi) = \mu^2|\psi|^2 - \lambda|\psi|^4 + \nu|\psi|^6, \quad (2)$$

with  $\mu$  representing the scalar field mass, and  $\lambda, \nu$  as positive parameters governing the self-interactions of the scalar field. We choose  $\mu = 1, \lambda = 200, \nu = 10000$ , defining the potential as  $V(\psi) = |\psi|^2 \left(1 - \frac{|\psi|^2}{0.1^2}\right)^2$ , which meets the energy condition and has degenerate minima at  $\psi = 0$  and  $|\psi| = 0.1$ .

Within this framework, we encounter RN black hole solutions characterized by total mass  $M$  and charge  $Q$ . Employing Painlevé-Gullstrand coordinates, we simulate the full nonlinear evolution of the RN black hole. As initial states, we set  $M_0 = 1, Q = 0.9$  which establish the energy scale for this study. We then impose an ingoing initial scalar perturbation to the seed RN black hole:

$$\psi_0 = pr^3 \left(1 - \frac{r}{r_1}\right)^3 \left(\frac{r}{r_2} - 1\right)^3, \text{ if } r \in [r_1, r_2], \quad (3)$$

and zero otherwise. We set  $r_1 = 8, r_2 = 12$  and vary the amplitude  $p$ . The initial perturbation is neutral, keeping the total charge of the system unchanged, while the total mass increases with amplitude  $p$ . Other initial conditions have also been explored, yielding consistent qualitative results. Additional details regarding the numerical setup can be found in the Supplemental Material.

## III. NONLINEAR SUPERRADIANT INSTABILITY

We monitor key physical variables throughout the evolution, including the scalar field value  $\psi_h$  on the apparent horizon, the scalar field energy  $E_\psi$  and charge  $Q_\psi$ ,

along with black hole charge  $Q_h$  and irreducible mass  $M_h = \sqrt{S_h/16\pi}$ , computed from the apparent horizon area  $S_h$ . While charge and energy are transferred from and to the black hole, we confirm that the charge conservation  $Q_\psi + Q_h = Q$  persists well, and the irreducible mass of the black hole does not decrease throughout the evolution. Our studies reveal that all RN black holes remain stable against small perturbations, despite experiencing superradiance. Only significantly large perturbations can trigger the transition of an RN black hole into a hairy black hole. We term this novel phenomenon as nonlinear superradiant instability. It differs from linear superradiant instability, which leads to a transition to a hairy black hole even with the slightest perturbation, as observed in scenarios involving RN black holes confined by an artificial mirror [16] or in AdS space [17].

By varying the gauge coupling parameter  $q$ , we explore the characteristic dynamic features of the nonlinear superradiant instability of RN black holes under moderate perturbations with amplitude  $p = 0.5$ , resulting in an increased total mass  $M = 1.183$ . In Fig.1, we observe that for small  $q$  (e.g.,  $q = 3$ ), despite the initial extraction of charge from the black hole to the scalar field, the black hole fully reabsorbs the charge as time progresses. Ultimately, the scalar field is nearly completely absorbed by the central black hole, resulting in an enlarged bald RN solution as the end state.

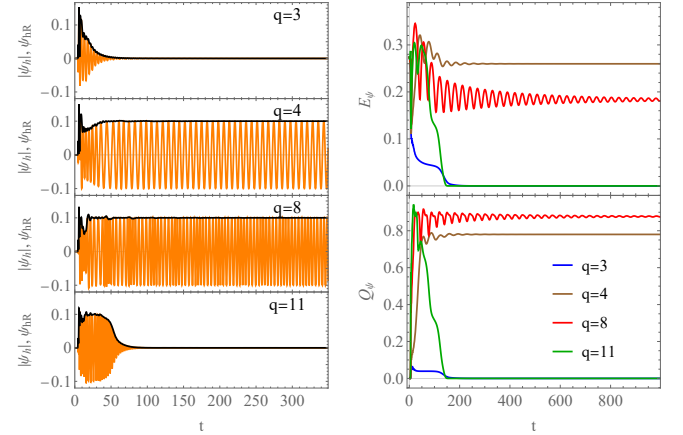


Figure 1. Evolution of quantities for  $q = 3, 4, 8, 11$  with perturbation amplitude  $p = 0.5$ . Left panel: the absolute scalar field value  $|\psi_h|$  on the horizon (black) and the real part  $\psi_{hR}$  (orange). The imaginary part  $\psi_{hI}$  follows a similar behavior to  $\psi_{hR}$ , but with a phase difference of  $\pi/2$  at late times. Right panel: the scalar field energy  $E_\psi$  and charge  $Q_\psi$ . The black hole charge  $Q_h$  follows curves overlapping with those for  $Q - Q_\psi$ .

As  $q$  increases to an intermediate range (e.g.  $q = 4, 8$ ), a bald RN black hole can be destroyed, resulting in a final state characterized by a black hole with nontrivial scalar hair. The real and imaginary components of the complex scalar field exhibit oscillations with frequencies  $\omega = qA_H$ , where  $A_H$  represents the gauge potential at the horizon when the system reaches complete equilibrium. This re-

sult validates the novel Q-hairy black hole solutions found in [6, 10]. Throughout the evolution, the scalar field energy experiences periodic growth and decline, akin to the bosenova phenomenon seen in Kerr black holes [23, 24] and confined RN black holes [16–18] due to linear superradiant instability. However, the underlying mechanism differs because in our case, the RN black hole keeps stable under linear perturbations. This conclusion finds support in the charge behavior during the evolution. Initially, a significant amount of charge transfers from the black hole to the scalar field. Nevertheless, a fraction of charge is pushed back to the black hole and can be extracted once again. This cyclic process persists over an extended duration, particularly evident for larger  $q$ . It contrasts with the previously observed bosenova scenario where charge extraction is never reversed [16]. In essence, here the bounces of scalar energy and charge arise from the interplay between the extraction due to superradiance and the absorption stemming from gravity and self-interaction. We suggest a connection between this phenomenon and the energy enhancement mechanism inherent in the periodically oscillating complex scalar hair surrounding the black hole, akin to discussions regarding Q-balls [25, 26]. Further clarity may be achieved through future linear analysis. For larger  $q$ , the final Q-hairy black hole approaches a neutral Schwarzschild black hole adorned with Q-hair. This transition results from the nearly complete extraction of charge from the seed RN black hole to the surrounding scalar field over time.

As  $q$  increases further (e.g.,  $q = 11$ ), the extraction of charge and energy from the black hole becomes notably more vigorous, to the extent that it can even invert the black hole charge to be negative. Nevertheless, both the extracted charge and energy are eventually reabsorbed by the central black hole, culminating in a bald RN black hole with an increased mass. This contrasts sharply with the case of linear superradiant stability, which results in a more robust development of scalar hair for larger  $q$  [16].

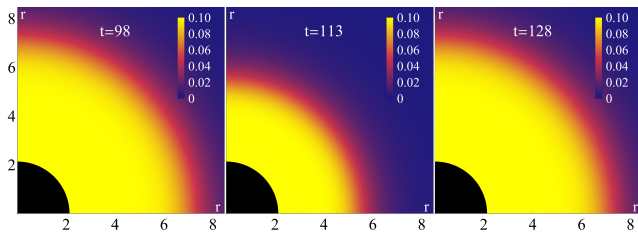


Figure 2. The snapshots of the absolute value  $|\psi|$  of the scalar field when  $q = 8$  and  $p = 0.5$ . The radial contraction and expansion corresponds to the alternation between dense and sparse patterns in the evolution of  $\psi_{hR}$  for  $q = 8$  depicted in Fig.1.

Before reaching the final Q-hairy black hole solution for intermediate  $q$ , a fascinating phenomenon emerges: the scalar field surrounding the black hole undergoes prolonged expansion and contraction during its evolution, as visualized in Fig.2. This phenomenon resembles the radial oscillations in relativistic stars [27], but is disclosed

for the first time in a black hole system. These radial oscillations closely align with the temporal pattern observed in the extraction and restoration of charge and energy by the scalar field, as illustrated in Fig.1. It is worth noting that the spatial expansion and contraction of the scalar field imply a time-dependent geometry that has not yet stabilized. In each cycle, a small amount of the scalar field energy and charge is absorbed by the central black hole. When complete equilibrium is reached, a Q-hairy black hole forms, with its complex scalar hair undergoing temporal oscillations, while its energy-momentum tensor and geometry remain static.

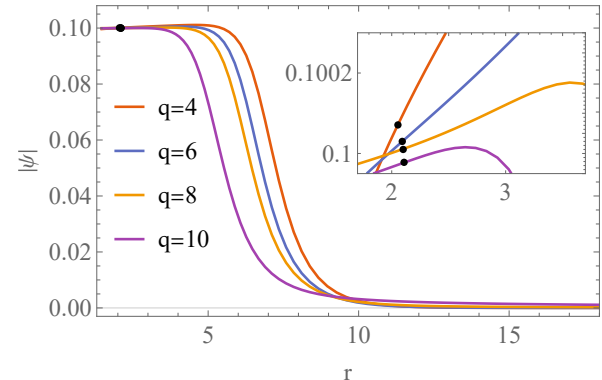


Figure 3. The ultimate distribution of Q-hair for different  $q$  when  $p = 0.5$ , with the black hole horizon positions indicated by the black spots in the inset. A small peak of the scalar field occurs beyond the horizon, attributed to the non-zero scalar mass.

In Fig.3, we depict the ultimate distribution of the black hole Q-hair for various  $q$ . Irrespective of  $q$ , the Q-hair consistently exhibits domain wall behavior. Near the black hole, the scalar field is confined to the vacuum state with  $|\psi| = 0.1$ . Moving away from the black hole, the scalar field gradually transitions to the vacuum state with  $|\psi| = 0$ . For larger  $q$ , the Q-hair approaches closer to the black hole, while also displaying a more pronounced tail in the remote region.

#### IV. CRITICAL DYNAMICS

In addition to the fully nonlinear superradiant process driving the transition from linearly stable bald black holes to hairy ones, we have discovered intriguing dynamical critical behaviors near the transition thresholds. In our numerical study with fixed  $q = 8$  for the initial perturbation (3), we surprisingly identified four distinct amplitude thresholds  $p_n$ , as illustrated in Fig.4. Depending on amplitude  $p$ , the final solution falls into one of two categories: a Q-hairy black hole for  $p_1 < p < p_2$  or  $p_3 < p < p_4$ , or a bald RN black hole for other  $p$ . Importantly, all physical quantities in the final state exhibit abrupt changes around these thresholds, indicating type I dynamical critical behaviors [19–22, 28].

Critical solutions emerge precisely at the thresholds,

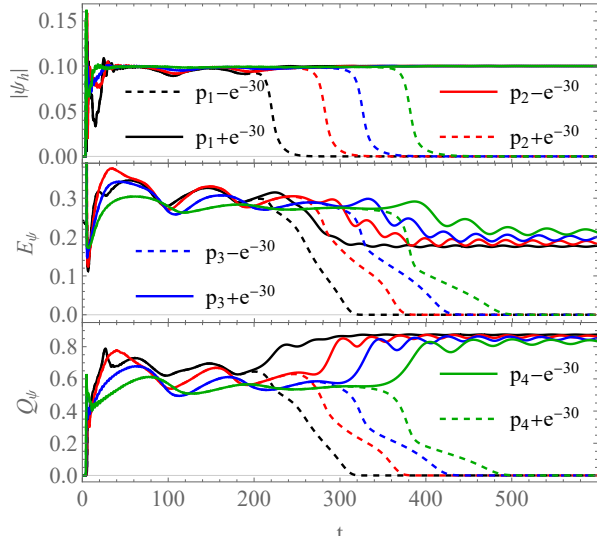


Figure 4. Evolution of the scalar field absolute value  $|\psi_h|$  on the apparent horizon, its energy  $E_\psi$  and charge  $Q_\psi$  for varying amplitudes  $p$  with  $q = 8$ . The solid curves correspond to the evolution resulting in Q-hairy black holes, while the dashed curves correspond to the evolution resulting in RN black holes. The thresholds  $p_1 = 0.46846497920368$ ,  $p_2 = 0.74574104807946$ ,  $p_3 = 0.93694909507780$ , and  $p_4 = 1.10804525511232$  have been precisely determined with an accuracy of  $10^{-14}$  using the bisection method. The first few digits remain consistent despite potential numerical influences.

representing linearly unstable hairy black holes that act as attractors in the evolution. As  $p$  approaches these thresholds, we observe that all intermediate solutions exhibit a prolonged proximity to the critical solutions. This duration can be quantified as  $T_n = -\omega_{nI}^{-1} \ln |p - p_n|$  with  $\omega_{nI}$  representing the imaginary part of the unstable mode ( $\omega_n = \omega_{nR} + i\omega_{nI}$ ) corresponding to the critical solution at threshold  $p_n$ . Specifically, we have  $\omega_{1I} = 0.127$ ,  $\omega_{2I} = 0.107$ ,  $\omega_{3I} = 0.0926$ , and  $\omega_{4I} = 0.0763$ . It is worth noting that these unstable modes possess a non-zero real part  $\omega_{nR}$ . This discovery introduces a novel mechanism for the type I critical dynamical transition, distinct from the previously identified tachyonic instability which always has a vanishing real part of the unstable mode in the Einstein-Maxwell-scalar theory [19–21] and extended scalar-Gauss-Bonnet theory [22]. On the other hand, although we find that this new instability satisfies the superradiant condition and can extract energy and charge from the black hole, it differs significantly from the typical linear superradiant instability. For instance, RN black holes can have multiple unstable superradiant modes [17, 18], whereas critical solutions leading to type I dynamical critical behaviors always have just one unstable mode [28]; a real scalar perturbation cannot trigger the superradiant instability of an RN black hole, but any perturbation can initiate the inherent instability of the critical solution discussed here; the nonlinear evolution

of the typical superradiant instability always results in charge and energy extraction from the central black hole, whereas in our scenario, as the critical solution evolves into a bald RN black hole, both the charge and energy of the scalar field are drawn into the central black hole. To better understand this new instability, further research, particularly linear perturbation analysis, is needed.

As the critical solutions evolve towards the ultimate Q-hairy black holes, only a fraction of the scalar energy is absorbed by the central black hole, meanwhile the black hole charge is released into the Q-hair. In contrast to the ultimate Q-hairy black holes, the critical solutions exhibit less charge and greater scalar energy outside the black hole. On the apparent horizon, all final Q-hairy black holes exhibit  $|\psi_h| = 0.1$ . Interestingly, the critical solutions also consistently demonstrate  $|\psi_h| = 0.1$ . Both the critical solutions and the final Q-hairy black hole solutions manifest scalar hair that expands and contracts within space before the system achieves equilibrium.

## V. DISCUSSION

We have uncovered a novel dynamic mechanism governing the transition between bald and hairy black holes. This mechanism arises from a fully nonlinear superradiant process, distinct from the linear superradiant instability. During the evolution, the scalar hair exhibits radial expansion and contraction, accompanied by rhythmic fluctuations in scalar field energy and charge. This phenomenon, reflecting a new type of bosenova, is observed for the first time in a black hole system, surpassing the explanation offered by linear superradiant instability. We have revealed new type I dynamical critical behaviors near the transition thresholds, where the critical solution displays an inherent linear instability, distinct from the previously observed tachyonic instability [19–22].

Beyond the charged black holes discussed, analogous dynamical phenomena are anticipated in rotating black holes [29, 30]. The fully nonlinear rotating bosenova holds significant potential for astrophysical interests. These phenomena should also manifest in black holes with other types of solitary hair, such as Proca and axion hair [1, 9]. The mass and self-interaction of the hair play crucial roles in naturally confining and sustaining stable hairy solutions in asymptotically flat spacetime, eliminating the need for artificial mirrors or AdS boundaries.

## ACKNOWLEDGMENTS

This work is supported by the Natural Science Foundation of China (NSFC) under Grants No. 11975235, 12005077, 12035016, 12075202, and 12375048, as well as the Guangdong Basic and Applied Basic Research Foundation under Grant No. 2021A1515012374.

---

[1] R. Brito, V. Cardoso, and P. Pani, *Superradiance: New Frontiers in Black Hole Physics*, Lect. Notes Phys., **906**, pp.1 (2015), arXiv:1501.06570 [gr-qc].

[2] W. H. Press and S. A. Teukolsky, *Floating Orbits, Superradiant Scattering and the Black-hole Bomb*, Nature, **238**, 211 (1972).

[3] V. Cardoso and P. Pani, *Testing the nature of dark compact objects: a status report*, Living Rev. Rel., **22**, 4 (2019), arXiv:1904.05363 [gr-qc].

[4] C. A. R. Herdeiro and E. Radu, *Kerr black holes with scalar hair*, Phys. Rev. Lett., **112**, 221101 (2014), arXiv:1403.2757 [gr-qc].

[5] S. Hod, *Stability of the extremal Reissner-Nordström black hole to charged scalar perturbations*, Phys. Lett. B, **713**, 505 (2012), arXiv:1304.6474 [gr-qc].

[6] J.-P. Hong, M. Suzuki, and M. Yamada, *Spherically Symmetric Scalar Hair for Charged Black Holes*, Phys. Rev. Lett., **125**, 111104 (2020), arXiv:2004.03148 [gr-qc].

[7] A. E. Mayo and J. D. Bekenstein, *No hair for spherical black holes: Charged and nonminimally coupled scalar field with selfinteraction*, Phys. Rev. D, **54**, 5059 (1996), arXiv:gr-qc/9602057.

[8] S. R. Coleman, *Q-balls*, Nucl. Phys. B, **262**, 263 (1985), [Addendum: Nucl.Phys.B 269, 744 (1986)].

[9] S. L. Liebling and C. Palenzuela, *Dynamical boson stars*, Living Rev. Rel., **26**, 1 (2023), arXiv:1202.5809 [gr-qc].

[10] C. A. R. Herdeiro and E. Radu, *Spherical electro-vacuum black holes with resonant, scalar Q-hair*, Eur. Phys. J. C, **80**, 390 (2020), arXiv:2004.00336 [gr-qc].

[11] S. R. Dolan, *Instability of the massive Klein-Gordon field on the Kerr spacetime*, Phys. Rev. D, **76**, 084001 (2007), arXiv:0705.2880 [gr-qc].

[12] W. E. East and F. Pretorius, *Superradiant Instability and Backreaction of Massive Vector Fields around Kerr Black Holes*, Phys. Rev. Lett., **119**, 041101 (2017), arXiv:1704.04791 [gr-qc].

[13] W. E. East, *Massive Boson Superradiant Instability of Black Holes: Nonlinear Growth, Saturation, and Gravitational Radiation*, Phys. Rev. Lett., **121**, 131104 (2018), arXiv:1807.00043 [gr-qc].

[14] C. A. R. Herdeiro, J. C. Degollado, and H. F. Rúnarsson, *Rapid growth of superradiant instabilities for charged black holes in a cavity*, Phys. Rev. D, **88**, 063003 (2013), arXiv:1305.5513 [gr-qc].

[15] S. R. Dolan, S. Ponglertsakul, and E. Winstanley, *Stability of black holes in Einstein-charged scalar field theory in a cavity*, Phys. Rev. D, **92**, 124047 (2015), arXiv:1507.02156 [gr-qc].

[16] N. Sanchis-Gual, J. C. Degollado, P. J. Montero, J. A. Font, and C. Herdeiro, *Explosion and Final State of an Unstable Reissner-Nordström Black Hole*, Phys. Rev. Lett., **116**, 141101 (2016), arXiv:1512.05358 [gr-qc].

[17] P. Bosch, S. R. Green, and L. Lehner, *Nonlinear Evolution and Final Fate of Charged Anti-de Sitter Black Hole Superradiant Instability*, Phys. Rev. Lett., **116**, 141102 (2016), arXiv:1601.01384 [gr-qc].

[18] N. Sanchis-Gual, J. C. Degollado, C. Herdeiro, J. A. Font, and P. J. Montero, *Dynamical formation of a Reissner-Nordström black hole with scalar hair in a cavity*, Phys. Rev. D, **94**, 044061 (2016), arXiv:1607.06304 [gr-qc].

[19] C.-Y. Zhang, Q. Chen, Y. Liu, W.-K. Luo, Y. Tian, and B. Wang, *Critical Phenomena in Dynamical Scalarization of Charged Black Holes*, Phys. Rev. Lett., **128**, 161105 (2022), arXiv:2112.07455 [gr-qc].

[20] C.-Y. Zhang, Q. Chen, Y. Liu, W.-K. Luo, Y. Tian, and B. Wang, *Dynamical transitions in scalarization and descalarization through black hole accretion*, Phys. Rev. D, **106**, L061501 (2022), arXiv:2204.09260 [gr-qc].

[21] J.-Y. Jiang, Q. Chen, Y. Liu, Y. Tian, W. Xiong, C.-Y. Zhang, and B. Wang, *Type I critical dynamical scalarization and descalarization in Einstein-Maxwell-scalar theory* (2023), arXiv:2306.10371 [gr-qc].

[22] Y. Liu, C.-Y. Zhang, Q. Chen, Z. Cao, Y. Tian, and B. Wang, *The critical scalarization and descalarization of black holes in a generalized scalar-tensor theory* (2022), arXiv:2208.07548 [gr-qc].

[23] A. Arvanitaki and S. Dubovsky, *Exploring the String Axiverse with Precision Black Hole Physics*, Phys. Rev. D, **83**, 044026 (2011), arXiv:1004.3558 [hep-th].

[24] H. Yoshino and H. Kodama, *The bosenova and axiverse*, Class. Quant. Grav., **32**, 214001 (2015), arXiv:1505.00714 [gr-qc].

[25] P. M. Saffin, Q.-X. Xie, and S.-Y. Zhou, *Q-ball Superradiance* (2022), arXiv:2212.03269 [hep-th].

[26] V. Cardoso, R. Vicente, and Z. Zhong, *On energy extraction from Q-balls and other fundamental solitons* (2023), arXiv:2307.13734 [hep-th].

[27] K. D. Kokkotas and J. Ruoff, *Radial oscillations of relativistic stars*, Astron. Astrophys., **366**, 565 (2001), arXiv:gr-qc/0011093.

[28] C. Gundlach and J. M. Martin-Garcia, *Critical phenomena in gravitational collapse*, Living Rev. Rel., **10**, 5 (2007), arXiv:0711.4620 [gr-qc].

[29] C. Herdeiro, E. Radu, and H. Runarsson, *Non-linear Q-clouds around Kerr black holes*, Phys. Lett. B, **739**, 302 (2014), arXiv:1409.2877 [gr-qc].

[30] C. A. R. Herdeiro, E. Radu, and H. Rúnarsson, *Kerr black holes with self-interacting scalar hair: hairier but not heavier*, Phys. Rev. D, **92**, 084059 (2015), arXiv:1509.02923 [gr-qc].

## SUPPLEMENTAL MATERIAL

The Einstein equations, given as

$$R_{\mu\nu} - \frac{1}{2}g_{\mu\nu}R = 2T_{\mu\nu}^A + T_{\mu\nu}^\psi, \quad (4)$$

involve energy-momentum tensors

$$T_{\mu\nu}^A = F_{\mu\rho} F_{\nu}^{\rho} - \frac{1}{4} g_{\mu\nu} F_{\rho\sigma} F^{\rho\sigma}, \quad (5)$$

$$T_{\mu\nu}^{\psi} = \frac{1}{2} (D_{\mu}\psi)^* (D_{\nu}\psi) + \frac{1}{2} (D_{\mu}\psi) (D_{\nu}\psi)^* - \frac{1}{2} g_{\mu\nu} (D^{\mu}\psi (D_{\mu}\psi)^* + V). \quad (6)$$

The Maxwell equations, written as

$$\nabla_{\mu} F^{\mu\nu} = \frac{1}{4} iq (\psi^* D_{\mu}\psi - \psi (D_{\mu}\psi)^*) g^{\mu\nu} \equiv j^{\nu}, \quad (7)$$

introduce a conserved current  $j^{\nu}$  satisfying  $\nabla_{\mu} j^{\mu} = 0$ . The scalar equation

$$D^{\mu} D_{\mu}\psi = \frac{\partial V}{\partial |\psi|^2} \psi. \quad (8)$$

The model is invariant under a local  $U(1)$  gauge transformation  $A_{\mu} \rightarrow A_{\mu} + \partial_{\mu}\chi, \psi \rightarrow \psi e^{iq\chi}$ , where  $\chi$  is a regular real function of spacetime coordinate.

For dynamic simulation in spherically symmetric spacetime, we employ the Painlevé-Gullstrand (PG) coordinates:

$$ds^2 = -(1 - \zeta^2)\alpha^2 dt^2 + 2\alpha\zeta dt dr + dr^2 + r^2(d\theta^2 + \sin^2\theta d\phi^2). \quad (9)$$

Here  $\alpha, \zeta$  are metric functions dependent on  $t$  and  $r$ . This coordinate system, conformally flat spatially, remains regular at the apparent horizon  $r_h$  where  $\zeta(t, r_h) = 1$ .

We take the gauge potential  $A_{\mu} dx^{\mu} = Adt$ . Introducing auxiliary variables

$$\Phi = \partial_r \psi, \quad (10)$$

$$\Pi = \frac{1}{\alpha} (\partial_t \psi - iqA\psi) - \zeta \Phi, \quad (11)$$

$$B = \frac{1}{\alpha} \partial_r A, \quad (12)$$

The Einstein equations can be reduced to

$$0 = \partial_r \alpha + \frac{\alpha r \text{Re}(\Pi \Phi^*)}{2\zeta}, \quad (13)$$

$$0 = \partial_r \zeta + \frac{\zeta}{2r} - \frac{r}{4\zeta} (\Pi \Pi^* + \Phi \Phi^* + 2B^2 + V) - \frac{r}{2} \text{Re}(\Pi \Phi^*), \quad (14)$$

$$0 = \partial_t \zeta - \frac{1}{2} \alpha r \left[ \Pi \Pi^* + \Phi \Phi^* + \left( \zeta + \frac{1}{\zeta} \right) \text{Re}(\Pi \Phi^*) \right]. \quad (15)$$

The Maxwell equations give

$$0 = \partial_r B + \frac{2B}{r} - \frac{q}{2} \text{Im}(\Pi \psi^*), \quad (16)$$

$$0 = \partial_t B - \frac{q}{2} \alpha \text{Im} [(\zeta \Pi + \Phi) \psi^*]. \quad (17)$$

The scalar equation becomes

$$0 = \partial_t \Pi - \partial_r [\alpha (\Pi \zeta + \Phi)] - \frac{2\alpha(\Pi \zeta + \Phi)}{r} - iA\Pi q + \alpha \psi \frac{\partial V}{\partial |\psi|^2}. \quad (18)$$

By using initial scalar distribution  $\psi_0$  and  $\Pi_0$ , we derive initial  $\Phi, B$  from (10,16), respectively. Then initial  $\zeta, \alpha, A$  can be worked out from (14,13,12) successively. All the data on the initial time slice are acquired. Subsequently, we utilize evolution equations (15,18,11) to compute  $\zeta, \Pi, \psi$  on the next time slice, while solving the constraint equations (10,16,13,12) to determine  $\Phi, B, \alpha, A$  on the corresponding time slice. By repeating this procedure, metric and matter field data for all time slices are obtained.

### A. Physical quantities

We monitor the evolution of several quantities during our analysis: the scalar field energy  $E_\psi$ , scalar field charge  $Q_\psi$ , black hole charge  $Q_h$  and irreducible mass  $M_h = \sqrt{S_h/16\pi}$ , where  $S_h = 4\pi r_h^2$  represents the apparent horizon area. The scalar field energy is calculated as follows:

$$E_\psi = \frac{1}{4\pi} \int_{r_h}^{\infty} d^3x \sqrt{-\gamma} T_{\mu\nu}^\psi n^\mu n^\nu = \int_{r_h}^{\infty} dr \frac{r^2}{2} (V + \Pi^* \Pi + \Phi^* \Phi). \quad (19)$$

Note that the scalar field energy density is nonnegative, satisfying the weak energy condition. The scalar field charge is associated with the Noether charge for the conserved current  $j^\mu$ :

$$Q_\psi = - \int dV n_\mu j^\mu = \int_{r_h}^{\infty} \frac{q}{2} r^2 \text{Im}(\Pi \psi^*) dr, \quad (20)$$

where the normal vector  $n_a = (-\alpha, 0, 0, 0)$ . The black hole charge can be determined using the formula

$$Q_h = - \frac{1}{4\pi} \oint_{r_h} dS F^{\mu\nu} n_\mu s_\nu = - r^2 B|_{r_h}, \quad (21)$$

where  $s_\nu = (0, 1, 0, 0)$  is the outward pointing unit normal vector to the apparent horizon two-sphere. The total charge of the system is  $Q = Q_h + Q_\psi$ .

### B. Initial and boundary conditions

We choose the initial seed black hole to be a RN black hole with  $\alpha_0 = 1$  and  $\zeta_0 = \sqrt{\frac{2M_0}{r} - \frac{Q^2}{r^2}}$ . Here,  $M_0 = 1$  and  $Q = 0.9$  represent the total mass and charge of the black hole, respectively, and they serve as the energy scale for our study. Then we impose following ingoing initial scalar perturbation on the seed RN black hole:

$$\psi_0 = pr^3 \left(1 - \frac{r}{r_1}\right)^3 \left(\frac{r}{r_2} - 1\right)^3, \quad \text{if } r \in [r_1, r_2] \text{ and zero otherwise,} \quad (22)$$

$$\Pi_0 = \Phi_0 = \partial_r \psi_0. \quad (23)$$

We fix  $r_1 = 8, r_2 = 12$  and vary the amplitude  $p$ . The initial perturbation is neutral such that the total charge of the system remains unchanged, while the total mass increases with amplitude  $p$ . We have used other types of perturbation, such as a Gaussian wave. All the numerical results are qualitatively the same.

We specify following boundary condition for (13) to solve  $\alpha$  during the evolution:

$$\alpha|_{r \rightarrow \infty} = 1, \quad (24)$$

This particular choice of boundary condition stems from the auxiliary freedom of  $\alpha dt$  in PG coordinates and implies that an observer at infinity will measure time using the proper time coordinate  $t$ . We also require that

$$A, B, \Pi, \Phi|_{r \rightarrow \infty} = 0, \quad (25)$$

throughout the evolution. They imply that  $\partial_t \phi|_{r \rightarrow \infty} = \partial_t \Pi|_{r \rightarrow \infty} = 0$  in (11,18). These conditions are sensible as matter cannot reach spatial infinity in a finite amount of time.

As previously mentioned, we use (14) to solve for the initial values of  $\zeta$ . For this purpose, we specify the following boundary condition:

$$\zeta|_{t=0, r=r_c} = \zeta_0(r_c). \quad (26)$$

Here  $\zeta_0(r)$  refers to the metric function of the initial seed RN black hole, and  $r_c = 0.99r_{h0}$  denoting a cutoff located close to the initial apparent horizon  $r_{h0} = 1.436$  from the interior.

At asymptotic spatial infinity, there are

$$\zeta = \sqrt{\frac{2M}{r}} (1 + O(1/r)), \quad (27)$$

where  $M$  is the total mass. To improve the stability and accuracy, we use the variable  $s = \sqrt{r}\zeta$  in the code. After obtaining the initial  $\zeta$  or  $s$  using (14), we can calculate the total mass of the system via

$$M = \lim_{r \rightarrow \infty} \frac{r}{2} \zeta(t, r)^2. \quad (28)$$

During subsequent evolution, we fix

$$s|_{r \rightarrow \infty} = \sqrt{2M}. \quad (29)$$

This specification implies that we set  $\partial_t s|_{r \rightarrow \infty} = 0$  in (15) during the evolution.

### C. Numerical setup and convergence

We introduce a coordinate compactification with  $z = \frac{r}{r+5M_0}$ . The simulation takes place within  $z \in [z_c, 1]$ , where  $z_c = \frac{r_c}{5M_0+r_c}$  and  $z = 1$  represents spatial infinity. We discretize  $z$  uniformly using 2000 grid points. We employ fourth-order finite difference in the radial direction and fourth-order Runge-Kutta in the time direction. To stabilize the simulation, we apply the Kreiss-Oliger dissipation. In the first step, we use Newton-Raphson method to solve the constraint equation (14), employing L'Hospital's rule at  $z = 1$ .

We have assessed the accuracy and convergence of our numerical method in various ways. Convergence in the finite difference method is typically estimated as  $\frac{u_{2N} - u_N}{n_{4N} - n_{2N}} = 2^n + O(\frac{1}{N})$ , where  $u_N$  represents the results obtained with  $N$  grid points for evolutionary quantity  $u$ , and  $n$  is the order of accuracy. Please note that for a radial integration of fundamental evolution variables, the convergence order should be  $n - 1$ . Fig.5 displays the convergence of integral quantities (19,20), confirming the fourth-order convergence of our numerical method.

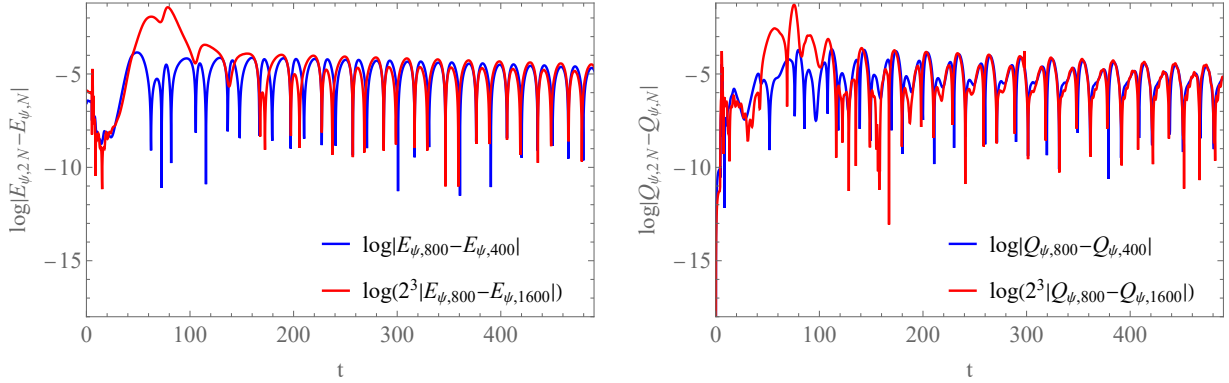


Figure 5. The convergence tests for scalar field energy (left) and charge (right) with  $N = 400$ , for the initial perturbation (3) with  $p = 0.5$  and  $q = 8$ , show that both  $\frac{E_{\psi,2N} - E_{\psi,N}}{E_{\psi,4N} - E_{\psi,2N}}$  and  $\frac{Q_{\psi,2N} - Q_{\psi,N}}{Q_{\psi,4N} - Q_{\psi,2N}}$  are approximately  $2^3$ , indicating our numerical method has convergence order of  $n = 4$ .